ORIGINAL PAPER

Realization of vibronic entanglement in terms of tunneling current in an artificial molecule

Kinshuk Banerjee · Gautam Gangopadhyay

Abstract Based on the concept of molecular nonadiabatic processes, namely, curve crossing and electronic interstate coupling, here we have introduced a model of an artificial molecule composed of three coupled quantum dots in terms of displaced harmonic oscillators of the confinement potential. We have shown that the static and dynamic features of vibronic entanglement can be realized in terms of the tunneling current in our model. An entanglement sudden-death can be shown to be equivalent to the suppression of tunneling current at the appropriate parameters of the magnetic field. We have also provided the nonclassicality of the vibration of the dot confinement potential which maximizes at the anticrossing zone.

Keywords Tunneling current · Vibronic entanglement · Artificial molecule

1 Introduction

Energy level mixing and superposition of quantum states in atomic and molecular systems [1,2] are well-studied phenomena in physics. The modern research now focuses on the production of 'artificial atom' structures, called quantum dots [3,4], which act as tiny laboratories where the ideas and theories of many-body physics developed to understand atoms and nuclei can be applied and more importantly, can be controlled externally unlike real atoms or molecules [5–9]. Quantum dots are artificially

K. Banerjee
Department of Chemistry, University of Calcutta, 92 A.P.C. Road,
Kolkata 700009, India

G. Gangopadhyay (✉)
S.N. Bose National Centre for Basic Sciences, Block-JD, Sector-III,
Salt Lake, Kolkata 700098, India
e-mail: gautam@bose.res.in

designed low-dimensional nanometer-sized systems confined in all the three spatial dimensions with atom-like properties that can be filled with electrons (or holes) [10]. Coupled quantum dots thus act like molecular analogues in solid-state. Quantum dot molecules [6,7,9] find novel applications in modern optoelectronic devices and quantum information processing with some surprising properties, e.g., antibonding ground states [9,11,12] that can not be explained by simply visualizing these systems as rescaled versions of real atomic-molecular systems. These interesting features come into life mainly due to the ability to externally control the coherent tunnel coupling [13,14] between two dots by varying the separation of the dots or by applying electric or magnetic field [7,9] and a desired molecular wavefunction can be prepared. The realization of phenomena familiar in quantum and atom optics [15–18] like dark state formation [19], current rectification [20] and trapping of population of electronic state [21] are discussed in various occasions for level-mixing in a single quantum dot (intradot mixing) or in spatially separated quantum dots (interdot mixing).

In a quantum dot, the nuclear potential of a real atom is replaced by an artificially generated confinement potential generally modelled as a two-dimensional anisotropic harmonic-oscillator [10,22,23]. Theoretical Fock–Darwin spectrum [24,25] of the quantum dot with an effective circular or elliptical and parabolic lateral confinement potential [10] shows exact level crossings [26] of the single-particle states evolving with the magnetic field. Level-mixing in molecules can be performed through coupling between different electronic states arising out of nonadiabatic processes. To analyze the analogous aspect of electronic interstate coupling or non-Born–Oppenheimer coupling of real molecules in an artificial molecule composed of coupled quantum dots, here we have theoretically studied the superposition of single particle states of different dots in an interdot mixing scheme.

Single as well as coupled quantum dots are ideal systems to study the generation, control and the effects of quantum entanglement of excitons and electron pairs [5,6,27–32] on the experimentally realizable properties [33,34] which are essential ingredients of quantum information processing [35,36]. In the spirit of the above studies, in this paper we have considered an interdot coupling scheme of three single particle levels in three separate quantum dots with a suitable model Hamiltonian. This type of coupled three-dot structure have been studied in various situations with varying complexity [19,21,26,37,38]. The three coupled dots, which act collectively as the collector (or downstream) dot system is probed by an emitter (or upstream) dot. In the present setup of interdot level mixing, we have studied the entanglement between the electronic and the center-of-mass motional degrees of freedom where the motion is under the two-dimensional anisotropic harmonic-oscillator potential representing the dot confinement. In what follows we will simply call this center-of-mass motion due to confinement potential as vibration. The entanglement of the vibronic quantum state of the coupled quantum dots is measured in terms of the von Neumann entropy of entanglement [39,40]. We have also characterized the nonclassicality of the vibration corresponding to the dot confinement potential using the Wigner function matrix [41]. As the experimental realization of quantum entanglement is very challenging, here we have explored the connection between the variation of entanglement and the experimentally measurable tunneling current both in the steady state situation and also through their dynamical evolution at various magnetic field strengths.

In what follows we have described the model Hamiltonian for the interdot mixing in Sect. 2. The measures of entanglement and nonclassicality are given in Sect. 3. The numerical results are discussed in Sect. 4. The paper is concluded in Sect. 5.

2 Model for interdot mixing

The stationary states of an electron in a two-dimensional lateral anisotropic parabolic confinement potential, $V_c(x,y)$ in presence of a magnetic field along the z-direction are eigenstates of the Hamiltonian [24,25]

$$H = \frac{1}{2m^*}\left[\mathbf{p} - \frac{e}{c}\mathbf{A}\right]^2 + V_c(x,y), \tag{1}$$

where $\mathbf{A}$ is the symmetric gauge vector potential taken as $\mathbf{A} = \frac{1}{2}B(-y, x, 0)$ where B is the magnetic field and $V_c(x,y) = \frac{1}{2}m^*(\omega_x^2 x^2 + \omega_y^2 y^2)$ with m^* being effective electron mass. In this scenario the motion in the x-y plane is quantized with the energy eigenvalues given as

$$E_{n_x,n_y} = (n_x + 1/2)\hbar\omega_1 + (n_y + 1/2)\hbar\omega_2 \tag{2}$$

where ω_1, ω_2 are functions of ω_x, ω_y and ω_c where $\omega_c = eB/m^*c$ is the cyclotron frequency. n_x, n_y are the quantum numbers of the two-dimensional harmonic oscillator potential that acts as the mean-field confinement potential [10]. In absence of the magnetic field, $\omega_c = 0$ and then the energy levels are simply of a two-dimensional harmonic oscillator. On the other hand, for a high field strength with $\omega_c \gg \omega_x, \omega_y$ the energy levels are given by $E_{n_x} = (n_x + 1/2)\hbar\omega_c$, i.e., the Landau levels [10]. For the isotropic case with $\omega_x = \omega_y = \omega$, we have

$$\omega_1 = \left(\omega^2 + \frac{\omega_c^2}{4}\right)^{1/2} + \frac{\omega_c}{2} \tag{3}$$

and

$$\omega_2 = \left(\omega^2 + \frac{\omega_c^2}{4}\right)^{1/2} - \frac{\omega_c}{2}. \tag{4}$$

Here we consider three single particle levels undergoing mixing which are in three separate coupled quantum dots. The energy levels of the dots can be tuned and the tunneling barrier between two dots can be controlled by proper application of gate voltages [38] that, for example, can convert a cyclic triple quantum dot molecule to a linear one and vice versa. The three dots-1,2,3 are represented by the state vectors $|1\rangle$, $|2\rangle$ and $|3\rangle$ where $|1\rangle$ denotes the single electron to be on dot-1 etc. (see Fig. 1). The level mixing in the coupled dots is probed with another dot (emitter dot) in its ground state by bringing their energy levels selectively into resonance with adjusting the gate potential. Now if the two-dimensional confinement potential of the coupled dots is identical to that of the probe or emitter dot, then non-zero overlap is possible only between single particle states of emitter and collector dots with same set of quantum numbers n_x, n_y. But tunneling current measurements indicate finite overlap between the emitter dot ground state and high energy states of collector dot. It indicates that the confinement potentials are not identical for emitter and collector dots and energy
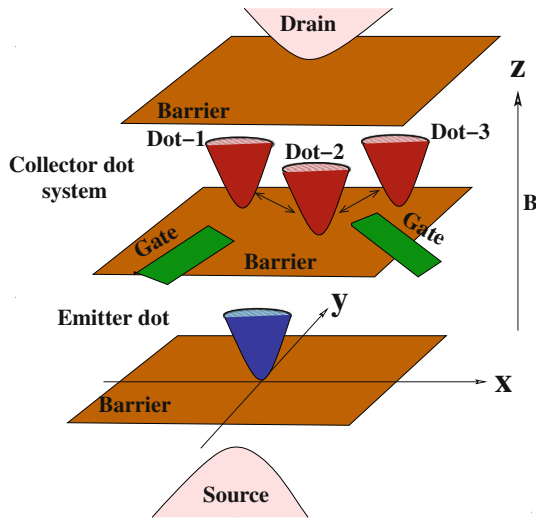
Fig. 1 Schematic diagram showing the interdot coupling situation. Here the collector dot system consists of three dots coupled in a linear arrangement which is probed with an emitter dot. The coupling between the dots is shown with a *double-headed arrow*. Each dot is represented with its two-dimensional confinement potential shown in the cartoon in the x-y plane. The positions of the potential minima of the coupled dots in x-y plane are displaced compared to that of the emitter dot whose potential minimum is taken as the origin. B is the external magnetic field applied in z-direction. The energy levels of the dots and coupling among them can be controlled by properly placed gates (see Ref. [38]) two of which are shown in the picture for example. The triple barrier structure can be of made of materials like GaAs. Current flows through the system on application of a bias voltage between source and drain and gate voltages. The tunnel coupling between the emitter dot and the collector dot system is taken to be negligibly small

level mixing occurs due to coupling. Recent experimental result on three level mixing in a quantum dot [26] explains this in terms of the nonideal nature of the harmonic potential which is akin to anharmonic mode-mode couplings in molecules. Now this coupling can also be generated by electronic means via tunnel coupling between two dots forming a dot molecule. Here we model the coupling among three dots, that act collectively as the collector dot system, in the latter mechanism which we call interdot mixing. Although the effect of mixing of three single particle levels is qualitatively similar whether the mixing is intradot or interdot, we mention that the mechanism of energy sharing is significantly different in two cases.

We describe the emitter dot and the coupled collector dot system using a common set of vibrational coordinates with the confinement potential of each collector dot being represented as a displaced harmonic oscillator with respect to the emitter dot whose potential minimum is taken as the origin. Now the tunnel coupling among the dots is sufficient to give the level mixing. But we treat the collector dots with displaced oscillator potentials compared to the emitter dot for two reasons as follows. (1) Generally two dots in a nanodevice are of different size, composition and experience diverse strain fields [7,9] and hence should be modelled differently. (2) The displaced oscillator Hamiltonian when polaron transformed gives a tunnel coupling which is a function of the magnetic field and hence can reproduce the externally controlled interaction between two dots achieved experimentally. The Hamiltonian for the composite collector dot system is written in second quantization as ($\hbar = 1$)

$$H = \sum_{n=1}^{3} |n\rangle \left(\sum_{k=1}^{2} \left(\omega_k (a_k^\dagger a_k + 1/2) + g_{nk}(a_k^\dagger + a_k) + \frac{g_{nk}^2}{\omega_k} \right) \right) \langle n|$$

$$+ \sum_{\substack{n,\,m=1 \\ n \neq m}}^{3} |n\rangle V_{nm} \langle m|. \tag{5}$$

Here $a_k^\dagger$, a_k are the creation and annihilation operators of the harmonic confinement potential, g_{nk} is the vibronic coupling constant, V_{nm} is the interdot tunnel coupling matrix element and ω_k is the vibrational frequency given in Eqs. (3) and (4).

Applying a polaron transformation [42–45] on the Hamiltonian in Eq. (5) we get

$$\tilde{H} = \sum_{n=1}^{3} |n\rangle \left(\sum_{k=1}^{2} \left(\omega_k(a_k^\dagger a_k + 1/2) \right) \right) \langle n| + \sum_{\substack{n,\,m=1 \\ n \neq m}}^{3} |n\rangle V_{nm} \prod_{k=1}^{2} D_k(\alpha_{nmk}) \langle m|. \tag{6}$$

Here $D_k(\alpha_{nmk})$ is the Glauber displacement operator defined as $D_k(\alpha_{nmk}) = \exp\left(\alpha_{nmk}(a_k^\dagger - a_k) \right)$ where $\alpha_{nmk} = \frac{g_{nk} - g_{mk}}{\omega_k}$. Hence the off-diagonal elements of the Hamiltonian giving rise to the level mixing are magnetic field dependent. We solve the Hamiltonian in Eq. (6) to get the energy Ω_j and the eigenvectors of the collector dot system from $\tilde{H}|\psi^j\rangle = \Omega_j |\psi^j\rangle$ where the jth eigenstate of the composite collector dot system can be expressed as

$$|\psi^j\rangle = \sum_{l=1}^{3} \sum_{n_x,n_y=0}^{\infty} C_l^j |l, n_x, n_y\rangle. \tag{7}$$

The expansion coefficients depend on the vibrational coordinates corresponding to the confinement potential.

3 Measures of entanglement and nonclassicality

3.1 von Neumann entropy

The entanglement between the electronic and vibrational degrees of freedom of the composite states of the collector dot can be expressed using the von Neumann entropy of entanglement [39,40,46,47] as

$$E = -\mathrm{Tr}_{el}\left(\rho_{el} \log_3 \rho_{el} \right) = -\sum_k \gamma_k \log_3 \gamma_k. \tag{8}$$

Here ρ_{el} is the reduced density operator for the electronic degree of freedom (with three-dimensional state space) obtained by taking partial trace over the vibrational

degree of freedom of the total density operator ϱ i.e., $\rho_{el} = \text{Tr}_{vib}[\varrho]$. γ_k are the eigenvalues of ρ_{el}. The total density operator ϱ for the jth eigenstate of the system is constructed from Eq. (7).

Now the von Neumann entropy [40] for the system is defined as S $=$ $-\text{Tr}_{el}(\rho_{el}\log\rho_{el})$. For unentangled states the entropy is zero and so is E. On the other hand, the maximally entangled state with state space of dimensionality D has the maximum entropy log D [40]. So for the electronic degree of freedom with three electronic states, the maximum entropy will be log 3 and the maximum entanglement will be E = 1.

3.2 Wigner function matrix

Wigner function is a phase space quasiprobability distribution [48,49] that gives the complete information about the motional state of the system equivalent to the information contained in the corresponding density operator. Wigner function matrix [41] is the extended form of Wigner function to describe the composite system including the electronic degrees of freedom. It is useful for the complete description of the entangled electronic and vibrational motion [41,50] of the molecular system studied. By appropriate measuring techniques [51–55] the Wigner function can be an index of quantum interference and one can realize the quantum state of a given system.

The Wigner function matrix for the superposed states of the coupled collector dot system can be written as [50]

$$W_{ij}(\beta_1, \beta_2) = \text{Tr}\left[\varrho A_{ji}\delta(\beta_1 - a_1)\delta(\beta_2 - a_2)\right]. \tag{9}$$

Here ϱ is the total density operator describing the electronic and vibrational degrees of freedom. A_{ji} is the electronic flip operator given by $A_{ji} = |j\rangle\langle i|$ that gives rise to transition from state $|i\rangle$ to state $|j\rangle$. β_i $(i=1,2)$ represents the complex phase space amplitude of the vibrational motion defined as $\beta_i = (Q_i + iP_i)$ with Q_i being the dimensionless normal vibrational coordinate of the ith mode and P_i its conjugate momentum. $\delta(\beta_i - a_i)$ is the operator-valued delta function [49] defined as the Fourier transform of the displacement operator $D(\xi) = \exp(\xi a^\dagger - \xi^* a)$ as,

$$\delta(\beta_i - a_i) = \frac{1}{\pi^2}\int d^2\xi D(\xi)\exp\left(\beta_i\xi^* - \beta_i^*\xi\right)$$
$$= \frac{2}{\pi}D(\beta_i)(-1)^{a_i^\dagger a_i}D^\dagger(\beta_i). \tag{10}$$

The Wigner function corresponding to the vibrational degree of freedom can be obtained from the Wigner function matrix by simply taking the trace over the electronic degree of freedom [41] and is given as

$$W(\beta_1, \beta_2) = \sum_i W_{ii}(\beta_1, \beta_2). \tag{11}$$

The negativity of the Wigner function reveals the nonclassicality of the vibrational motion and can also give an idea about the entanglement in the system [47]. A non-classical state gives rise to entangled output states when mixed with the vacuum [56] which is not the case with a 'classical' state. We define the nonclassicality of a particular eigenstate of the system by a parameter δ defined as the volume of the negative portion of the Wigner function [57] in the phase space of the vibrational motion in the confinement potential. It is given by

$$\delta = \int\limits_{Q_1,Q_2} \int\limits_{P_1,P_2} (|W| - W)\, dQdP, \qquad (12)$$

with $W = W(Q_1, Q_2, P_1, P_2)$ and $dQ = dQ_1 dQ_2$, $dP = dP_1 dP_2$.

4 Results and discussion

To show the applicability of the model Hamiltonian for interdot level mixing, we take the three states in three separate dots undergoing superposition. The states are denoted with their vibrational quantum numbers (n_x, n_y) as (0,5), (1,3) and (2,1). The jth eigenstate of the collector dot system then reduces to

$$|\psi^j\rangle = C_1^j|1, 0, 5\rangle + C_2^j|2, 1, 3\rangle + C_3^j|3, 2, 1\rangle, \quad j = 1, 2, 3. \qquad (13)$$

Here the basis state $|1, 0, 5\rangle \equiv |1\rangle \otimes |0, 5\rangle$ indicates the $|0, 5\rangle$ state in dot-'1' and similarly the other basis states are defined. The superposed states $|\psi^j\rangle$ are called lower branch state, middle branch state and upper branch state for j = 1, 2, 3, respectively. For the linear arrangement of the three collector dots we take $V_{13} = V_{31} = 0$. With this set up we have determined the tunneling current which is proportional to the overlap between the emitter or probe dot ground state and the molecular states of the coupled collector dot system given in Eq. (13). We have studied the variation of the tunneling current as a function of the external magnetic field and analyzed the relation between the tunneling current and the vibronic entanglement in the interdot mixing case in two different subsections giving results for steady state situation and dynamic evolutions of both the quantities.

4.1 Steady state

In this study the values of the parameters of the Hamiltonian in Eq. (6) are taken in such a way that produces the avoided crossing behavior in the energy evolution of the mixed states of the three collector dots as a function of the magnetic field as well as gives the field dependent tunneling current variation with suppression of the center branch current at a particular field strength. To numerically solve the interdot Hamiltonian (Eq. 6) for the energies and eigenvectors we take $\omega = 5.3$ meV and all the relevant parameters are scaled with respect to ω. We take the tunnel couplings V_{12} between collector dot-1 and dot-2 and V_{23} between dot-2 and dot-3 equal to

Fig. 2 Energy values of the coherent composite eigenstates of the coupled collector dot system are plotted as a function of the magnetic field. The *straight lines* denote the energy variation of the uncoupled basis states
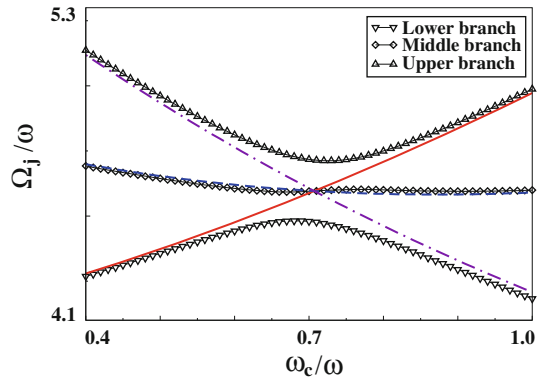
0.5 (scaled with respect to ω). The values of g_{nk} (see Eq. 5) are taken like this: $g_{11} = 2.1, g_{12} = 2.6, g_{21} = g_{22} = 1.5, g_{31} = 0.9$ and $g_{32} = 0$. This gives $\alpha_{121} = \alpha_{231} = 0.6, \alpha_{122} = 1.1$ and $\alpha_{232} = 1.5$. Here the coupling between the (0,5) (in dot-1) and (1,3) (in dot-2) basis states increases from 0.03 (scaled with respect to ω) at $\omega_c/\omega = 0.4$ to 0.06 at $\omega_c/\omega = 0.8$ and then decreases to 0.05 at $\omega_c/\omega = 1.0$. The coupling between the (1,3) and (2,1) (in dot-3) basis states increases from 0.025 to 0.08 in the same total range. We must point out that this choice of parameters is obviously not unique in giving the avoided crossing and current suppression.

The evolution of the energy and eigenvectors as a function of the magnetic field is studied. The variation of energy of the coupled states are shown in Fig. 2 as a function of the magnetic field. The avoided crossing of the states is clearly visible around $\omega_c/\omega = 0.71$ with a level splitting energy of ~ 1.1 meV. This value of ω_c corresponds to a magnetic field of 2.1T with $m^* = 0.065m_0$ where m_0 is the free electron mass. The value of m^* taken is typical for quantum dot devices. This result tallies well with the experimental findings of Payette et al. [26] where the energy levels are determined from the differential conductance resonance positions and explained theoretically with higher degree terms in the confinement potential of a single dot.

We calculate the individual branch currents I_j which are proportional to the overlap between the superposed states of the collector dot and the $1s$-like ($n_x = 0, n_y = 0$) ground state, $|G\rangle$ of the emitter dot acting as the probe. The Hamiltonian for the ground state is obtained from Eq. (5) with all the g_{nk} and V_{nm} values set equal to zero. The tunneling current through the jth eigenstate is given as [13,14]

$$I_j \propto |\sum_{i=1}^{3} C_i^j \chi_i|^2, \quad j = 1, 2, 3. \tag{14}$$

Here χ_i denotes the vibrational overlap of the emitter dot ground state with the high energy states of the collector dot system modelled as displaced harmonic oscillators. If the states $|n\rangle$ and $|m\rangle$ belong to two different oscillators with the oscillators being defined using the same vibrational coordinate with one oscillator being displaced with respect to the other by an amount α, the vibrational overlap $\langle n|m\rangle$ is defined as [42]

Fig. 3 The calculated branch currents of the coupled collector dot system are displayed as a function of the magnetic field
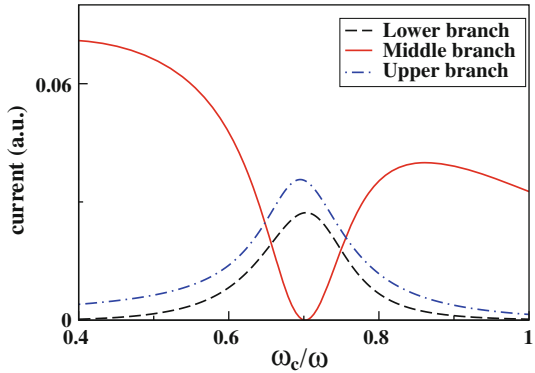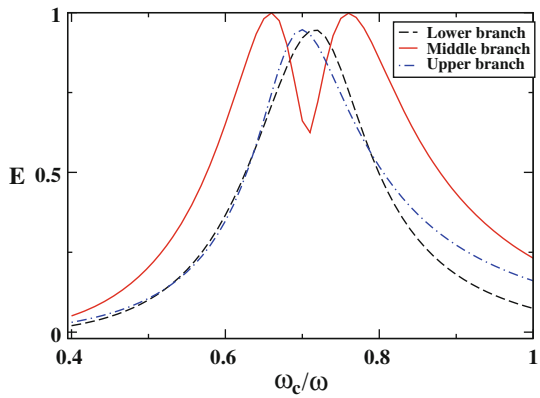

Fig. 4 The entanglement parameter, E plotted as a function of the magnetic field for the three branch states for the interdot coupling case

$$\langle n|m\rangle = \exp\left(\frac{-\alpha^2}{2}\right)\sqrt{\frac{m!}{n!}}\,\alpha^{n-m}L_m^{n-m}(\alpha^2). \tag{15}$$

Here $L_m^{n-m}(\alpha^2)$ is an associated Laguerre polynomial with real α. In our case of the two-dimensional confinement potential of the quantum dots, the above expression is easily extended [44]. The displacement parameter is given in terms of the vibronic coupling parameters g_{nk} (see Eq. 6). One can notice that Eq. (15) is equivalent to the Franck–Condon factor in vibronic spectra.

The current through the respective branch states arising out of superposition are plotted in Fig. 3 as a function of the magnetic field. From the figure we can see that the middle branch current undergoes a strong suppression at a value of $\omega_c/\omega \sim 0.71$ which is the anticrossing point. For both the upper and lower branch states, the respective currents rise to their maximum values at the same magnetic field region.

Now we measure the entanglement between the electronic and vibrational degrees of freedom as a function of the magnetic field for the three branch states. The entanglement E is determined using Eq. 8 and plotted in Fig. 4. The connection between entanglement and the tunneling current becomes clear from Fig. 4. It is evident that close to the avoided crossing point, the entanglement for all the three states undergoes

Table 1 The magnetic field strengths (in units of ω), given in the parentheses, at which the tunneling currents, I_j and the vibronic entanglement, E become maximum or minimum for all the superposed states

Branch state	I_j (a.u.)	E
Lower ($j = 1$)	0.02727 (0.703)	0.947 (0.715)
Middle ($j = 2$)	$\sim 10^{-7}$ (0.703)	0.615 (0.707)
Upper ($j = 3$)	0.03567 (0.695)	0.947 (0.699)

a significant change. For the lower and upper branch states, E passes through a maximum at $\omega_c/\omega \sim 0.71$. It is the same point around which the current through these states become maximum also. For the middle state, the variation of E shows a split maximum with two more or less symmetric peaks around $\omega_c/\omega = 0.71$ and hence a local minimum at this point corresponding to the minimum in the current. So there is a nice correspondence between the current variation and the variation in E. This type of connection between entanglement and the measured current is already indicated in similar systems of coupled quantum dots [33,34]. But we emphasize that the vibronic entanglement studied here is different from those studies as it focuses specifically on the role of the confinement potential. We have given the magnetic field strengths (in units of ω) at which the tunneling currents and the vibronic entanglement become maximum or minimum for all the superposed states in Table 1. The important fact is that tunneling current measurement experiments in double or triple coupled quantum dots can give useful information about the effect of this type of entanglement on the current intensity which will be of prime importance in quantum information processing devices.

To illustrate the robustness of the connection between current and entanglement variations, next we vary one of the g_{nk} parameters, namely, g_{11} over the range 1.51–3.0 around its initially taken value of 2.1. Then α_{121} varies from 0.01 to 1.5. We study the most interesting current variation, i.e., suppression of the current for the middle branch state over this parametric variation. One can see from the left panel of Fig. 5 that the current suppression around $\omega_c/\omega = 0.71$ is a robust feature present for all the different g_{11} values with the position of the minimum current being shifted towards a slightly lower magnetic field for lower g_{11} e.g., the zero current position is at $\omega_c/\omega = 0.68$ for $g_{11} = 1.51$.

Although the current suppression position do not change much with the parameter variation, the slope of the fall and rise of the current changes significantly with the slope being higher for lower value of g_{11}. For $g_{11} = 1.51$, the current falls sharply above $\omega_c/\omega = 0.67$, becomes zero at $\omega_c/\omega = 0.68$ and then rises very slowly being close to zero up to $\omega_c/\omega = 0.74$. Then at $\omega_c/\omega = 0.75$ it shoots up rapidly, goes through a maximum and then falls off gradually as is the case with other values of the parameter. But interestingly for $g_{11} = 1.51$ there is an extended region of the magnetic field over which the current is very low and the current variation in this zone ($\omega_c/\omega = 0.68 - 0.74$) is qualitatively different from other g_{11} values. The variation of g_{11} corresponds to different positioning of one of the collector dots in the device with respect to the emitter dot. Hence this result can be very important in the context of the dependence of the current on device fabrication and hence its external control.
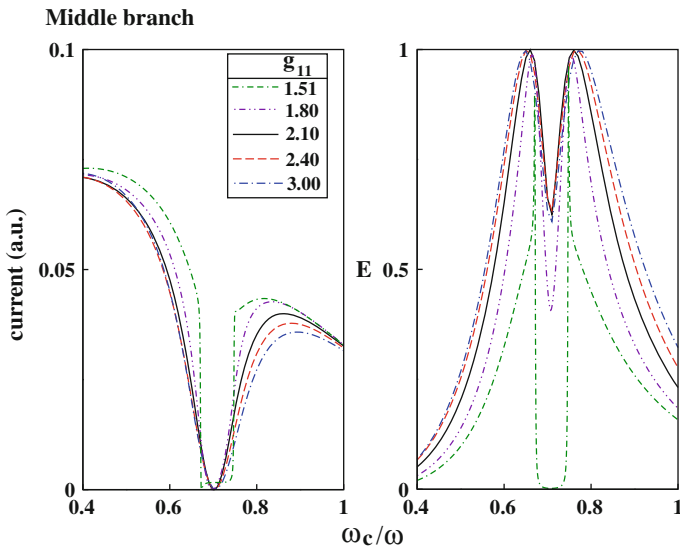
Fig. 5 Effect of variation of the vibronic coupling parameter g_{11} (keeping other parameters fixed) on the current through the middle branch state and the corresponding entanglement

Here also we calculate the variation of entanglement between the electronic and vibrational subsystems with the magnetic field for different values of g_{11} to see how the correspondence between current and entanglement gets affected. From the right panel of Fig. 5 we can easily see that the split maximum in the entanglement, E around the local minimum at $\omega_c/\omega = 0.71$ remains to be the distinctive feature of the middle branch state. For higher g_{11}, the two peaks in the E variation curve get slightly shifted away from the $\omega_c/\omega = 0.71$ point whereas for the lower range of g_{11} they come closer with the deep in the entanglement at $\omega_c/\omega = 0.71$ getting bigger. The case of $g_{11} = 1.51$ is again interesting here as in this case the two peaks in the E variation curve are almost needle-like with extremely sharp rise and fall of E. The highly important feature here is the sudden death of entanglement over the same zone of the magnetic field ($\omega_c/\omega = 0.68 - 0.74$) where the tunneling current is also very low. The corresponding relations between the current and the entanglement variation for upper and lower branch states also continue to be valid (not shown in figures) over the parametric variation. Hence we conclude that the relation between the tunneling current and vibronic entanglement is a genuine feature. In the next section we will explore whether this connection between the current and the entanglement survives in the dynamical evolution of the system.

Before that we give the variation of the nonclassicality parameter, δ (see Eq. 12), corresponding to the vibrational degree of freedom of the confinement potential, as a function of the magnetic field plotted in Fig. 6 for the three branch states of the coupled collector dots. We see that δ passes through a maximum for all the states and the maximum is at $\omega_c/\omega = 0.71$ for the middle state and around it for the other two states (at $\omega_c/\omega = 0.68$ for the lower state and $\omega_c/\omega = 0.73$ for the upper state). This indicates the mixing of the energy levels at this magnetic field range. But unlike the

Fig. 6 Variation of the nonclassicality parameter, δ as a function of the magnetic field for the three branch states of the coupled collector dots
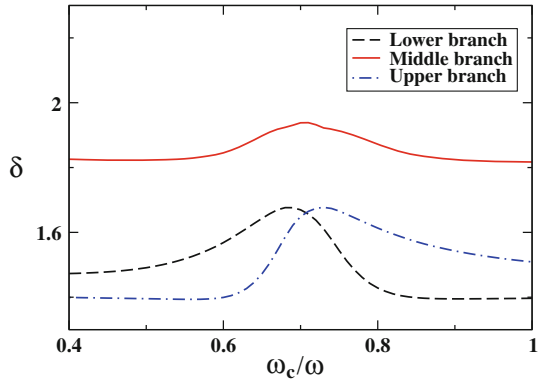
case of entanglement variation (see Fig. 4), there is no local minimum at or around this point for the middle branch state corresponding to the tunneling current suppression. This shows that the information of the phase relationship among the wavefunction coefficients gets lost in this case of nonclassicality evaluation. However we point out that Wigner function matrix formulation is successfully used by Vera et al. [58] in the characterization of dynamical regimes and entanglement sudden death in a microcavity quantum dot system.

4.2 Dynamical evolution

Here we have studied the dynamics of the current as well as the vibronic entanglement evolution by solving the time-dependent Schrödinger equation for three different magnetic fields, $\omega_c/\omega = 0.4, 0.71$ and 1.0. For each magnetic field, three initial conditions are chosen for the numerical solution of the dynamics. In condition (1), the initially populated state is $|1, 0, 5\rangle$, for condition (2) the initially populated state is $|2, 1, 3\rangle$ and for condition (3) it is the $|3, 2, 1\rangle$ state. These conditions can be realized by bringing the emitter ground state in resonance with respective superposed levels in the coupled collector dots by adjusting the grid voltage of the device. We will discuss the results in the following manner: the current evolutions for different initial conditions are analyzed at a particular magnetic field followed by a similar analysis of the entanglement dynamics and then these two dynamics are compared. The results are plotted in Fig. 7.

At $\omega_c/\omega = 0.4$, the currents for conditions (1) and (3) oscillate in phase whereas for condition (2) the current variation is $180°$ out-of-phase compared to (1) and (3). The maximum value of the current is also small in case of (1) and (3) [particularly in (3)] compared to (2) with the minimum of the current being zero for (3). In the corresponding entanglement dynamics, E oscillates in phase for all the three initial conditions with the maximum value of E depending on the initial condition and every condition showing the dynamical sudden death of entanglement periodically. Now comparing the current and entanglement evolution we see that for conditions (1) and (3) the current and entanglement oscillate in phase and for condition (2) they are $180°$
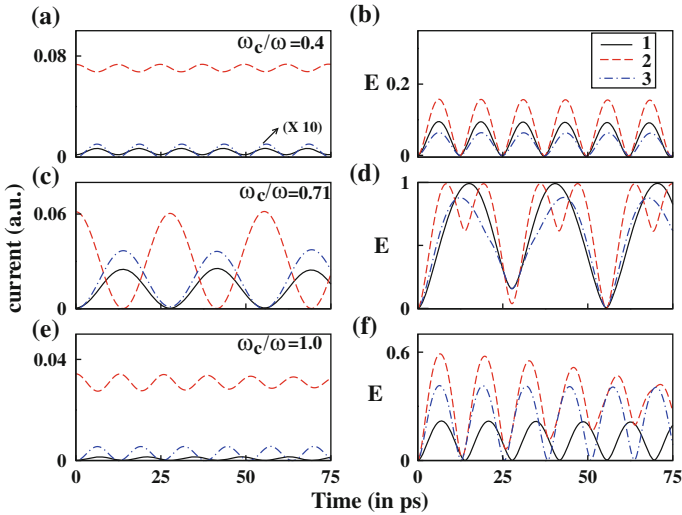
Fig. 7 Dynamic evolution of current and vibronic entanglement for three different magnetic fields: **a**, **b** $\omega_c/\omega = 0.4$, **c**, **d** $\omega_c/\omega = 0.71$ and **e**, **f** $\omega_c/\omega = 1.0$. **a**, **c**, **e** describe the current evolution with each plot showing results for three different initial conditions-1,2,3 described in the text. **b**, **d**, **f** show the corresponding entanglement variations

out-of-phase [34]. Hence the connection between the current and the entanglement is present also in the dynamical evolution with the specific relation being dependent on the initial condition.

Next we study the dynamics at the magnetic field $\omega_c/\omega = 0.71$ where the current maximizes for the upper and lower branch states and minimizes for the middle state in the steady state. Now in the dynamical study, the relation among the currents obtained for the three initial conditions remains the same as in the case with $\omega_c/\omega = 0.4$ but here the minimum value in the current oscillation becomes zero for all the initial conditions. In the entanglement evolution the in phase relation is present at the sudden death regions for all the initial conditions. In the region of maximum entanglement ($E \sim 1.0$) though, the oscillations are slightly out-of-phase for (1) and (3). For condition (2), we get the split maximum with two peaks instead of a single peak as in (1) and (3) which was the case also in the steady state study. Then for conditions (1) and (3), the current and entanglement oscillate more or less in phase particularly near the minima and they are slightly out-of-phase near the maxima. For condition (2), the current maxima are associated with the entanglement minima and the current minima are associated with the local minima in entanglement arising out of the split maxima.

For the case of $\omega_c/\omega = 1.0$, the interrelations are a bit more complicated. For (1) and (3), the current oscillations become gradually out-of-phase and become 180° out-of-phase at $t \sim 85$ time unit. The current oscillation in (2) is 180° out-of-phase compared to (3) and hence it is initially 180° out-of-phase compared to (1) but gradually the phase difference diminishes. There is a very interesting feature in the current evolution for condition (2) at this magnetic field which is not present in any of the other scenarios. The current oscillation for condition (2) actually shows an overall decay or collapse of its oscillations over the time range studied. Now as we come

to analyze the corresponding entanglement variation we find a similar collapse in the evolution of E for condition (2) with a 180° out-of-phase relation with the current. For conditions (1) and (3) also, we get a similar E evolution with the oscillations for the two conditions gradually becoming out-of-phase that finally become 180° out-of-phase. This feature is again similar to the corresponding current variation. Hence in this case also, for initial conditions (1) and (3) the current oscillates in phase with the entanglement and for initial condition (2) they are of opposite phase.

5 Conclusion

We have studied the mixing of three single particle levels in three separate coupled dots in an interdot mixing scheme where the profile of the energy levels as a function of the external magnetic field shows avoided crossing. We have determined the tunneling currents from the overlap of the emitter dot ground state and the superposed states of the collector dots and obtained the current suppression at the anticrossing zone for a particular delocalized molecular state of the coupled dots.

In the spirit of molecular nonadiabatic processes, the entanglement between the electronic and vibrational degrees of freedom of the dot confinement potential is determined for all the conditions under which the current variation is explored. Comparison of the results both in steady state and in time-dependent situation brings out a remarkable resemblance between the current and vibronic entanglement variations particularly in the manner in which these two quantities achieve their maxima and minima, i.e., their phase relation. This relation is maintained to a significant degree of accuracy over a large variation of the magnetic field and also for time evolution over tens of picoseconds. Parametric variation of one of the vibronic coupling constants illustrates the robust connection between current suppression behavior and the entanglement sudden-death over a narrow range of magnetic field strength. As different values of the vibronic coupling constant indicate varying displacements depending on the controllable magnetic field of the confinement potential, it can be very important in producing arbitrary nonadiabatic molecular features in an artificial system which are otherwise fixed by the real molecular parameters.

References

1. A. Nitzan, Ann. Rev. Phys. Chem. **52**, 681 (2001)
2. S. Mukamel, *Principles of Nonlinear Optical Spectroscopy* (Oxford University Press, NY, 1995)
3. M.A. Kastner, Rev. Mod. Phys. **64**, 849 (1992)
4. L.P. Kouwenhoven, T.H. Oosterkamp, M.S. Danoesastro, M. Eto, D.G. Austing, T. Honda, S. Tarucha, Science **278**, 1788 (1997)
5. G. Chen, N.H. Bonadeo, D.G. Steel, D. Gammon, D.S. Katzer, D. Park, L.J. Sham, Science **289**, 1906 (2000)
6. M. Bayer, P. Hawrylak, K. Hinzer, S. Fafard, M. Korkusinski, Z.R. Wasilewski, O. Stern, A. Forchel, Science **291**, 451 (2001)
7. H.J. Krenner, M. Sabathil, E.C. Clark, A. Kress, D. Schuh, M. Bichler, G. Abstreiter, J.J. Finley, Phys. Rev. Lett. **94**, 057402 (2005)
8. E.A. Stinaff, M. Scheibner, A.S. Bracker, I.V. Ponomarev, V.L. Korenev, M.E. Ware, M.F. Doty, T.L. Reinecke, D. Gammon, Science **311**, 636 (2006)

9. M.F. Doty, J.I. Climente, M. Korkusinski, M. Scheibner, A.S. Bracker, P. Hawrylak, D. Gammon, Phys. Rev. Lett. **102**, 047401 (2009)
10. S.M. Reimann, M. Manninen, Rev. Mod. Phys. **74**, 1283 (2002)
11. G. Bester, A. Zunger, J. Shumway, Phys. Rev. B **71**, 075325 (2005)
12. J.I. Climente, M. Korkusinski, P. Hawrylak, Phys. Rev. B **78**, 115323 (2008)
13. R. Landauer, IBM J. Res. Dev. **1**, 223 (1957)
14. S. Datta, *Electronic Transport in Mesoscopic Systems* (Cambridge University Press, Cambridge, 1997)
15. T. Vorrath, T. Brandes, Phys. Rev. B **68**, 035309 (2003)
16. B. Deb, G. Gangopadhyay, D.S. Ray, Phys. Rev. A **48**, 1400 (1993)
17. A. Bandyopadhyay, G. Gangopadhyay, J. Mod. Opt. **43**, 487 (1996)
18. K. Bergmann, H. Theuer, B.W. Shore, Rev. Mod. Phys. **70**, 1003 (1998)
19. C. Emary, Phys. Rev. B **76**, 245319 (2007)
20. K. Ono, D.G. Austing, Y. Tokura, S. Tarucha, Science **297**, 1313 (2002)
21. B. Michaelis, C. Emary, C.W.J. Beenakker, Europhys. Lett. **73**, 677 (2006)
22. M. Ghosh, R.K. Hazra, S.P. Bhattacharyya, Chem. Phys. Lett. **388**, 337 (2004)
23. M. Ghosh, R.K. Hazra, S.P. Bhattacharyya, J. Theor. Comput. Chem. **5**, 25 (2006)
24. V. Fock, Z. Phys. **47**, 446 (1928)
25. C.G. Darwin, Proc. Camb. Philos. Soc. **27**, 86 (1930)
26. C. Payette, G. Yu, J.A. Gupta, D.G. Austing, S.V. Nair, B. Partoens, S. Amaha, S. Tarucha, Phys. Rev. Lett. **102**, 026808 (2009)
27. W.D. Oliver, F. Yamaguchi, Y. Yamamoto, Phys. Rev. Lett. **88**, 037901 (2002)
28. P. Zhang, C.K. Chan, Q. Xue, X. Zhao, Phy. Rev. A **67**, 012312 (2003)
29. C.W.J. Beenakker, C. Emary, M. Kindermann, J.L. van Velsen, Phys. Rev. Lett. **91**, 147901 (2003)
30. A.D. Greentree, J.H. Cole, A.R. Hamilton, L.C.L. Hollenberg, Phys. Rev. B **70**, 235317 (2004)
31. G.M. Nikolopoulos, D. Petrosyan, P. Lambropoulos, Europhys. Lett. **65**, 297 (2004)
32. S. Yang, M. Gong, C. Li, X. Zou, G. Guo, Phy. Rev. B **80**, 235322 (2009)
33. E. del Valle, F.P. Laussy, C. Tejedor, Europhys. Lett. **80**, 57001 (2007)
34. J. Liu, Z. Jiang, B. Shao, Phy. Rev. B **79**, 115323 (2009)
35. L. Robledo, J. Elzerman, G. Jundt, M. Atatüre, A. Högele, S. Fält, A. Imamoglu, Science **320**, 772 (2008)
36. A. Kolli, B.W. Lovett, S.C. Benjamin, T.M. Stace, Phys. Rev. B **79**, 035315 (2009)
37. D.S. Saraga, D. Loss, Phys. Rev. Lett. **90**, 166803 (2003)
38. M. Korkusinski, I. Puerto Gimenez, P. Hawrylak, L. Gaudreau, S.A. Studenikin, A.S. Sachrajda, Phys. Rev. B **75**, 115301 (2007)
39. M.A. Nielsen, I.L. Chuang, *Quantum Computation and Quantum Information* (Cambridge University Press, Cambridge, 2000)
40. S. Stenholm, K.-A. Suominen, *Quantum Approach to Informatics* (Wiley, New York, 2005)
41. S. Wallentowitz, R.L. de Matos Filho, W. Vogel, Phys. Rev. A **56**, 1205 (1997)
42. V. May, O. Kuhn, *Charge and Energy Transfer Dynamics in Molecular Systems* (Wiley-VCH, Weinheim, 2004)
43. E.R. Bittner, S. Karabunarliev, L.M. Herz, J. Chem. Phys. **126**, 191102 (2007)
44. K. Banerjee, G. Gangopadhyay, J. Chem. Phys. **130**, 084705 (2009)
45. K. Banerjee, G. Gangopadhyay, Phys. Rev. B **81**, 035307 (2010)
46. S. Parker, S. Bose, M.B. Plenio, Phys. Rev. A **61**, 032305 (2000)
47. J.P. Dahl, H. Mack, A. Wolf, W.P. Schleich, Phys. Rev. A **74**, 042323 (2006)
48. S.M. Barnett, P.M. Radmore, *Methods in Theoretical Quantum Optics* (Clarendon Press, Oxford, 1997)
49. K.E. Cahill, R.J. Glauber, Phys. Rev. **177**, 1882 (1969)
50. S. Wallentowitz, R.L. de Matos Filho, S.C. Gou, W. Vogel, Eur. Phys. J. D **6**, 397 (1999)
51. T.J. Dunn, I.A. Walmsley, S. Mukamel, Phys. Rev. Lett. **74**, 884 (1995)
52. U. Leonhardt, Phys. Rev. A **55**, 3164 (1997)
53. C. Monroe, D.M. Meekhof, B.E. King, D.J. Wineland, Science **272**, 1131 (1996)
54. L.G. Lutterbach, L. Davidovich, Phys. Rev. Lett. **78**, 2547 (1997)
55. C. Kurtsiefer, R. Pfau, J. Mlynek, Nature **386**, 150 (1997)
56. A. Zavatta, V. Parigi, M. Bellini, Phys. Rev. A **75**, 052106 (2007)
57. A. Kenfack, K. Zyczkowski, J. Opt. B Quantum Semiclass. Opt. **6**, 396 (2004)
58. C.A. Vera, N. Quesada, H. Vinck-Posada, B.A. Rodriguez, J. Phys. Condens. Matter **21**, 395603 (2009)